Increased measurement range for spectral-domain optical coherence tomography through a moving reference mirror

Schouten, M.C.W.

Award date:
2019

Increased Measurement Range for Spectral-Domain Optical Coherence Tomography through a Moving Reference Mirror

Academic year 2018-2019

CST-number: CST2019.075

M.C.W. Schouten 0869793

Coach: ir. Y.G.M. Douven
Supervisor: dr. ir. M.J.G. v.d. Molengraft

University of Technology Eindhoven
Mechanical Engineering
Control Systems Technology
September 27, 2019

Increased Measurement Range for Spectral-Domain Optical Coherence Tomography through a Moving Reference Mirror

M.C.W. Schouten, Y.G.M. Douven and M.J.G. van de Molengraft
Department of Mechanical Engineering Eindhoven university of technology

Abstract In vitreo-retinal surgery, the required accuracy is often beyond what can be achieved by hand, especially for extended periods of time. To aid surgeons in reaching these accuracies, robotic systems have been developed. The surgeon views the patients retina through the pupil and therefore depth perception is limited. As a solution, an optical probe can be attached to the surgical instrument. Using spectral-domain optical coherence tomography (SD-OCT), one-dimensional depth-scans can be obtained. From these scans, distances from the surgical instrument tip to the retina can be acquired. However, the measurement range is currently limited to the size of the measurement window, which limits the set of measurable distances. This paper explores a method to increase the measurement range by automatically moving the start-position of the measurement window. A switching algorithm is developed to alternatively view and measure the position of the retina and the instrument tip, thereby keeping the maximum position variance bounded while improving safety through earlier distance measurements.

Nomenclature

K_k	Kalman gain value at iteration k.
N_x	Number of samples at component x.
P_k	Variance at iteration k.
Q_x	Model noise of component x.
R_x	Measurement noise on component x.
S_k	Innovation variance at iteration k
x_k	Position of x at iteration k.
$\tilde{y}_k$	Innovation at iteration k
σ_x	Standard-deviation of component x.

1 Introduction

In vitreo-retinal surgery procedures on the retina are performed. The retina is the light-sensitive layer in the back of the eye. To perform these procedures, high accuracy positioning of the surgical tool is required. This accuracy is often beyond what can be achieved by hand, especially for extended periods of time. To aid the surgeons in reaching these accuracies, surgical systems have been developed.

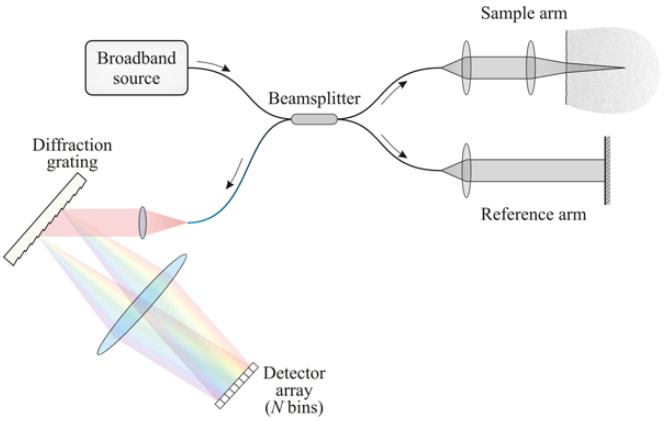

Fig. 1. Schematic oveview of the principle of SD-OCT [1].

Looking through a microscope, the surgeon observes the patients' retina through the pupil of the patient. Due to the small diameter of this pupil, between 1 and 8 millimeters [2], and the type of microscope used, depth-perception is limited. To provide the surgeon with axial distance information from the instrument to the retina, a relative distance sensor is added to the surgical system. An optical probe is integrated into the surgical instrument. Using spectral-domain optical coherence tomography (SD-OCT), one-dimensional depth images can be obtained. From these images, distances between detectable components can be obtained. This additional sensor can enhance safety during surgery as feedback becomes available. It also makes way for possible automated procedures.

Optical coherence tomography (OCT) is a non-invasive, high resolution interferometry technique that can be used to create one-dimensional depth images [3]. One particular OCT method is the SD-OCT, which is schematically shown in Fig. 1 [4]. In SD-OCT the light of a broadband optical light-source is split into two optical paths. One path leads to the sample, in this case the retina, the other path leads to a reference mirror. The interference of the light that is reflected from both paths is used to generate a one-dimension depth-scan. This depth-scan, called an A-scan, contains depth information over the span of the measurement window. The

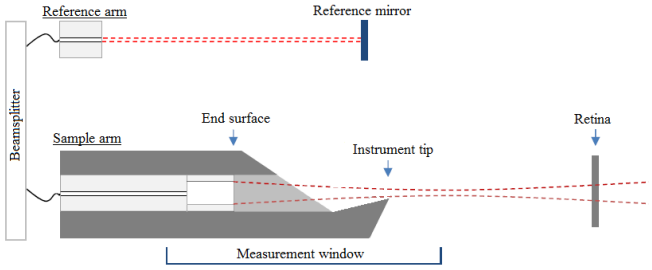

Fig. 2. Schematic overview of the relative positions of the end-surface, retina, instrument tip and measurement window in the the current set-up.

size and resolution of the measurement window depend on the wavelengths present in the light source and the amount of these wavelengths that the sensor can detect. A larger range of wavelengths applied, whilst keeping the amount of detectable wavelengths equal, results in a larger measurement window and a lower resolution.

Fig. 2 shows a schematic overview of the application of SD-OCT in a surgical system. The figure shows three essential components for measuring distances; the end-surface, instrument tip and the retina. The end-surface is the point where the light leaves the optical fiber and enters the environment. Due to the change in reflective index, the end-surface can be detected with the SD-OCT. The position of the instrument tip is essential to know, as this is the shortest distance from the instrument to the retina. If the instrument tip is not in the light path, it is not visible in the A-scans. In such cases, the distance between instrument tip and end-surface can be determined with a calibration if it is assumed that the probe, and thus also the end-surface, is rigidly connected to the surgical tool, and that the length of the surgical tool does not change during operation. The calibration of this distance can be done by touching an object with the instrument tip. When this object appears in the A-scan, the relative position of the instrument-tip to the end-surface can be calculated. Furthermore, Fig. 2 shows a possible position of the retina with respect to the instrument tip. This component is also detectable with the SD-OCT when within the measurement window. Thus knowing the positions of end-surface and retina, the axial distance from instrument tip to retina can be determined.

In the current set-up, the reference mirror is manually positioned such that the end-surface lies in the beginning of the measurement window, as is visible in Fig. 2. Although the end-surface position is fixed with respect to the surgical instrument, it is not necessarily fixed inside the A-scan. Changes in the path length of either sample arm or reference arm, result in a movement of the measurement window. Changes in path length can occur because of temperature change, stretching of the fiber due to pulling or movement and equipment vibration. As a result, the relative position of the end-surface inside the A-scan changes, while its position with respect to the fixed world does not.

Detecting the position of the end-surface in the A-scan is thus essential to accurately know estimate the axial distance from the instrument tip to the retina. Positioning the end-surface at the beginning of the measurement window, the distance at which the retina can be detected without the instrument tip touching it, is largest.

The SD-OCT device developed for the *Preceyes* surgical system has a limited measurement window of about 3.7 millimeter in water. Having a limited measurement window causes several performance limitations:

1. If due to malfunction of the sensor, either end-surface or retina is not detectable with the sensor, this can result in dangerous situations as it is unknown if the missing component is not detected or just not in the measurement window. It is assumed that the functioning of the sensor can only be validated when detecting the retina with the sensor, as the optical path to this component is longest. Currently this is not always possible as the measurement range is limited. Increasing the measurement range of the sensor would result in detecting the retina at larger distances, being able to validate sooner that the sensor is working.
2. During a surgery, a static- and dynamic model of the patients' eye is created. These models can be used to enhance safety by applying obtained knowledge of the shape and movements of the eye. These models are especially useful when high precision positioning with respect to the retina is desired. Due to the limited measurement window, only a limited range distances between end-surface and retina can be detected. The shape of the eye approximates a sphere with an inner diameter between 24 and 25 millimeter [2]. The result is that only for a small percentage of possible distances in the eye, actual distances can be measured, which limits the amount of data available to create the models. When the distance gets small and high precision position is desired, these models are still unreliable and can thus not yet be used. If the measurement range would be larger, information on the position and the movement of the retina would become available at larger distances. This makes it possible to create more reliable models before high precision positioning is desired.
3. For some surgical instruments it is not possible to position the instrument tip close to the end-surface, or even within measurement window distance of each other. As a result, the range of detectable distances decreases or even becomes zero. This limits the performance and makes the sensor even obsolete in the latter case. If the measurement range would be larger, the set of detectable distances increases. As a result, the sensor can be used for a larger variety of surgical instruments.

Each of these limitations are solved with a bigger measurement range. To accomplish this, an automatically moving reference mirror is introduced. Rather than making the measurement window larger at the cost of resolution, the measurement window can now be moved, thus leading to a larger range of positions on which components can be detected. A challenge here is to determine which component to position in the measurement window when it is not possible

to position end-surface and retina within the same measurement window.

This paper discusses a supervisor strategy for switching between the two detectable components (end-surface and retina) such that the mentioned limitations are resolved while keeping the variance on the distance from instrument tip to retina bounded. A switching strategy is developed in the form of an optimization problem. This is discussed in Section 2. To convert the optimization problem into a supervisor, models for tracking the positions of the two detectable components are required. These are discussed in Section 3. Section 4 elaborates on the periodic behavior that will occur when executing the strategy. Doing so will result in a set of equations that can be used to construct a supervisor. The supervisor is elaborated on in Section 5. The paper ends with a conclusion and recommendations in Section 8

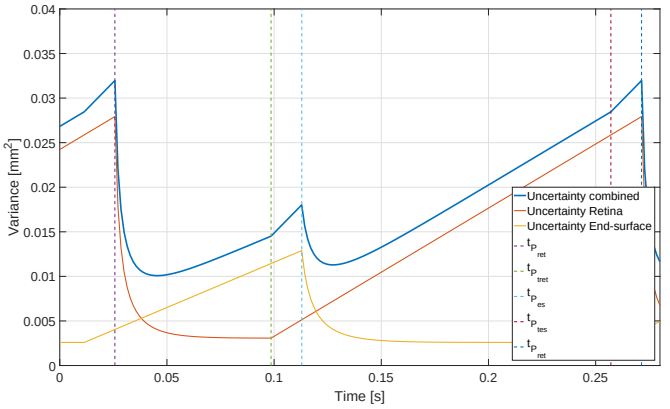

Fig. 3. Example periodic behavior of the variance. The figure shows the four stages of observing retina, traveling to end-surface, observing end-surface and traveling back

2 Strategy

Since it is possible that the end-surface and retina are not detectable within a single measurement window, altering the position of the reference mirror is required track the positions of both components. To determine when to position the reference mirror to observe the other component, a strategy for positioning the reference mirror needs to be developed. This strategy is formulated as an optimization problem. The solution of this optimization problem can be used to determine when to start positioning the reference mirror at the other component. In practice this means that a periodic behavior will occur. A full cycle through this behavior is called a period, which has a time-length t_p. A period consists of four parts, which start at time t_{p_x} inside a period:

1. $t_{p_{ret}}$: Retina is observed for first time after positioning the mirror. This part lasts for a certain time t_{ret} in which the retina is observed.
2. $t_{p_{tret}}$: The mirror moves to position the end-surface within the measurement window. This movement takes time t_{tt}.
3. $t_{p_{es}}$: The end-surface is observed for a certain time t_{es} after positioning the mirror.
4. $t_{p_{tes}}$: The mirror moves again to position the retina in the measurement window, also taking time t_{tt}.

An example of the changes in variance in a single period are shown in Fig. 3. The vertical lines here indicate the start of one of the parts.

To determine what should be optimized and under which conditions, the performance limitations mentioned in Section 1 are used:

1. Validating that the sensor is working as desired, is done by detecting the retina with the sensor. Since only the detections of the retina are required rather than a distance, there is no additional accuracy specification. The detection of the retina itself is thus sufficient to draw conclusions on the functioning of the sensor.
2. The modeling of the eye is composed of a dynamic- and static model. For the static model, distances from end-surface to retina are required. A small variance on this distance results in a more accurate measurement for the static model. As the dynamic model tries to model the movements of the two components. Assuming that the end-surface movements in the A-scan do not contains predictable dynamic behavior, only observing the retina is required as only relative movements of the retina are needed. Once a reliable dynamic model is obtained, it also becomes easier to construct a static model, as movements of the retina can be filtered out.
3. For each surgical instrument, and thus different distances for instrument tip to end-surface, safety must be ensured. Therefor it should always be guaranteed with a 99.99% certainty that the instrument tip is not touching the retina.

From these requirements it can be seen that observing the retina contributes in solving all three limitations. Observing the end-surface only helps in the construction of the static model and to keep the variance on the distance between tip and retina bounded. It is thus desired to maximize the percentage of time at the retina whilst keeping the variance on the distance between the instrument tip and retina bounded such that it can be guaranteed with 99.99% certainty that the instrument tip is not touching the retina. The percentage of time at the retina in a single period can be denoted as:

$$t_{\%ret} = \frac{t_{ret}}{t_{ret} + t_{es} + 2t_{tt}} \tag{1}$$

In this equation, $t_{\%ret}$ is the amount of time at the retina divided by the amount of time in a single period. To guarantee at each moment in time with 99.99% certainty that the distance from instrument tip to retina is larger than zero, the variance on this distance needs to be bounded. This can be written as:

$$P_{tip-ret} < \beta_{99.99\%}(\hat{D}_{tip-ret}) \tag{2}$$

In this equation, $P_{tip-ret}$ represents the variance on the dis-

tance from instrument tip to retina. $\beta_{99.99\%}$ represents the boundary on the variance for a 99.99% certainty bound, which is a function of the estimated distance from instrument tip to retina $\hat{D}_{tip-ret}$.

The complete optimization problem can be written as:

$$\begin{aligned} \min_{N_{ret},N_{es}} : \quad & \frac{1}{\bar{t}_{\%ret}} \\ s.t. : \quad & P_{tip-ret} < \beta_{99.99\%}(\hat{D}_{tip-ret}) \\ & t_{ret} < \alpha \\ & t_{es} < \gamma \\ For : \quad & T = \{t, ..., \infty\} \\ P.R. : \quad & N_{es}, N_{ret}, t_{\%ret}, \alpha, \beta, \gamma \in \mathbb{R}_{>0} \end{aligned} \tag{3}$$

Equation (3) shows the inverse of the average percentage of time at the retina over multiple periods, written as the parameter to minimize. Since it is required to optimize not just for a single period, but for all periods from the current time until infinite, the average is used to combine the percentages at the retina per period. The boundary condition on the distance variance is added and states that the variance at each moment in time, spanning from the current time to infinity, should remain bounded below a bound β, which is also time-dependent as $\hat{D}_{tip-ret}$ is time-dependent. A third and fourth boundary condition have been added as boundaries on the time at the retina and the time at the end-surface, as it may be desired to look at a component at least once in a certain time-frame. Furthermore the solution of this optimization problem, should guarantee that there also a feasible solutions for time going to infinite. This condition has to be added as the switching behavior in the current period, will influence the next and can possibly lead to an unfeasible solution in which it is not possible to meet the boundary conditions.

2.1 Boundary value

To obtain an expression for the boundary value β, Equation (4) is used.

$$\underbrace{\hat{D}_{es-ret} - \hat{D}_{tip-es}}_{\hat{D}_{tip-ret}} - \underbrace{t_{99.99\%}\sqrt{P}}_{D_{99.99\%}} > \tilde{D}_{mret} + \tilde{D}_{ms} \tag{4}$$

In this equation, $\hat{D}_{es-ret}$ denotes the estimated distance between the end-surface and retina. $\hat{D}_{tip-es}$ is the estimated distance from end-surface to instrument tip obtained from calibration. Combining both gives the estimated distance from instrument tip to retina. The sigma level for 99.99% multiplied by the square root of the variance gives the maximum distance from the estimated distance for 99.99% of time. To ensure the boundary value is not exceeded due to movements of retina or instrument, $\tilde{D}_{MRet}$ and $\tilde{D}_{MS}$ are added. These denote the possible movement of retina and instrument from manipulation by the surgeon, within a single samples. These are fixed parameters that are determined beforehand from analysis of the retina and maximum movement velocity of the surgical system.

The sigma level $t_{x\%}$ is the amount of multiplications of the standard-deviation that are required to cover a desired percentage of the distribution. The sigma level for 68.27 percent is thus equal to 1. Subtracting this distance from the expected distance from instrument tip to retina gives a value for the minimal distance with 99.99% certainty.

The estimated distance from instrument tip to retina minus the 99.99% distance of the estimated distance, should be larger than the $\tilde{D}_{mret}$ and $\tilde{D}_{ms}$, to ensure that the distance from instrument tip to retina is larger than zero in 99.99% of the cases. Rewriting Equation (4) leads to an expression for the boundary value β:

$$\beta_{99.99\%}(\hat{D}_{es-ret}) = \left(\frac{\tilde{D}_{mret} + \tilde{D}_{ms} - \hat{D}_{es-ret} + \hat{D}_{tip-es}}{t_{99.99\%}}\right)^2 \tag{5}$$

3 System

From the optimization problem it follows that it is required to estimate the distance from instrument tip to retina with a corresponding variance. These parameters can be used to determine the amount of time required to position the mirror to observe the other component, and to determine the 99.99% boundary value.

To determine this distance and variance it is required to track the positions of end-surface and retina with respect to each other. From analysis of the movements of both components from clinical trial data, an expression can be found for the movement of either component over time. The clinical trial data consists of surgery on five patients. The set of data concerns about 1.7 hours of logged data at a frequency of 700 hertz. The found model noise can then be used to update the variance of the components estimated position when it is not being observed. Furthermore, it is required to know the amount of time required to position the mirror to observe the other component. This value depends on the distance between the two components and the hardware used.

This section elaborates on the used implementation to determine expressions for the estimated distance and variance and how the time required to position the reference mirror can be determined.

3.1 Component model

To track the positions of end-surface and retina, a Kalman-filter is introduced for both components. A Kalman-filter is able to combine position measurements to estimate the actual position and gives a corresponding variance on this position [5]. The implemented Kalman filter is one-dimensional as the position that is desired to be tracked can be measured directly, and no model on the movement of either component is available [6]. For the latter reason, it is assumed that the position remains constant over time, giving the following equation for the predicated state estimate:

$$\hat{x}_{k|k-1} = \hat{x}_{k-1|k-1} \tag{6}$$

To prevent the variance on the position of one component having an influence on the measured position of the other component, the components' position has to be expressed in a frame where the distance between the components is not relevant. For this reason, absolute coordinates are not possible, as the absolute coordinate of the retina depends on the estimated position of the end-surface, which has an error. As a solution, each component position is expressed in terms of the reference mirror position. In this frame, the retina position is not dependent on the position of the end-surface as only the reference mirror position and position of the component in the A-scan are required. Besides the predicted state estimate, there is also a corresponding predicted estimate variance $P_{k|k-1}$:

$$P_{k|k-1} = P_{k-1|k-1} + Q_k \tag{7}$$

In this equation, $P_{k-1|k-1}$ is the updated estimate variance from the previous iteration. The model noise Q_k gives an expression for the possible movement of the component over time. This value is determined from position data from clinical trials. This analysis is discussed in Subsection 3.2. The innovation $\tilde{y}_k$ and innovation variance S_k become respectively:

$$\tilde{y}_k = z_k - \hat{x}_{k|k-1} \tag{8}$$

$$S_k = P_{k|k-1} + R_k \tag{9}$$

The measurement noise R_k for the innovation covariance for retina is determined in previous work, and is equal to 488 micrometer squared for an update frequency of 700 hertz [7]. This value is the combined result of normal distributions of heartbeat, measurement and breathing. Since changes in the optical path length occur, the position of the end-surface in reference mirror coordinates is not constant. Analysis of recorded end-surface positions during clinical trials resulted in a weighted average standard-deviation of 11.67 micrometer for the end-surface. The resulting measurement noise R_{es} thus becomes 136.19 micrometer if combined with the Gaussian noise of the measurement. Remarkable is that the results showed a possible dependency between movements of the end-surface and movements of the patient. All five patients from the clinical trials were under anesthesia, but one of the patients snored during the surgery, introducing movements of the retina. This patient showed a standard deviation of 19.0 micrometer on the end-surface movement, whereas the other four patients had an weighted average standard-deviation of 8.1 micrometer with a maximum value of 9.1 micrometer. Based on this it appears that the movement of the patient also influences the movement of the end-surface. However, due to the limited number of patients, this hypothesis can not be validated.

The Kalman gain K_k, updated state estimate $\hat{x}_{k|k}$ and updated state variance $P_{k|k}$ become respectively:

$$K_k = P_{k|k-1} S_k^{-1} \tag{10}$$

$$\hat{x}_{k|k} = \hat{x}_{k|k-1} + K_k \tilde{y}_k \tag{11}$$

$$P_{k|k} = (1 - K_k) P_{k|k-1} \tag{12}$$

The resulting estimated positions and variances of the two Kalman-filters can be combined to obtain the estimated distance from end-surface to retina, with a corresponding variance.

3.2 Retina and end-surface Analysis

To determine the model noise for the retina and end-surface, data from clinical trials is analyzed to get more insights into these movements and their occurrence rate. This subsection on finding expressions for these movements.

A window is defined as a subset of the total data. The size of this window, determines how much time the window covers. This amount of time is defined as a time-frame. The recorded position data of each component has been split up in overlapping windows. The overlap indicates that the start of a window lies within another window. A subset of the data in a window is thus also a subset of the data in another window. Creating windows with overlap from the total data of recorded position data, a set of windows can be obtained which all have the same time-frame. For analysis, the first point of each window is assumed to be the last known measurement. Using this value, the maximum occurring absolute delta with respect to this measurement value can be found per window. Doing so for each window results in a mapping, showing how often a certain discretized delta occurs within a certain time-frame. Normalizing this gives the occurrence rate of each delta.

This process can be repeated for various time-frames. The result is a map of the occurrence rates of various deltas for various time-frames. Combining these mappings for various patients, results in one large mapping of occurrence rates.

The occurrence rate for a certain time-frame can be summed up for increasing delta, until a desired occurrence coverage percentage $y\%$ is reached. The delta corresponding to the latest added occurrence rate shows the maximum delta includes $y\%$ of all occurring deltas. Calculating this delta for various values of$y\%$ and all time-frames for which windows were made, results in a set of maximum deltas. The obtained deltas as a function of $y\%$ and all time-frames are shown in Fig. 4 and Fig. 5. Assuming that the movement of the component can be modeled with a normal distribution, the standard-deviation can be determined as function of the time-length window and the percentage of occurrences

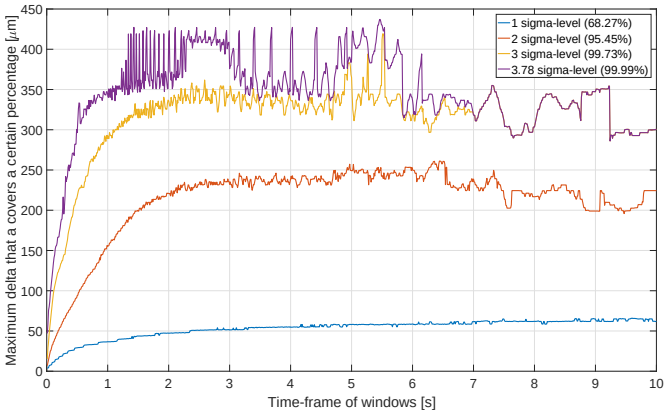

Fig. 4. Maximum occurring delta within an OCP of all occurrences for retina positions as a function of the time-length window size.

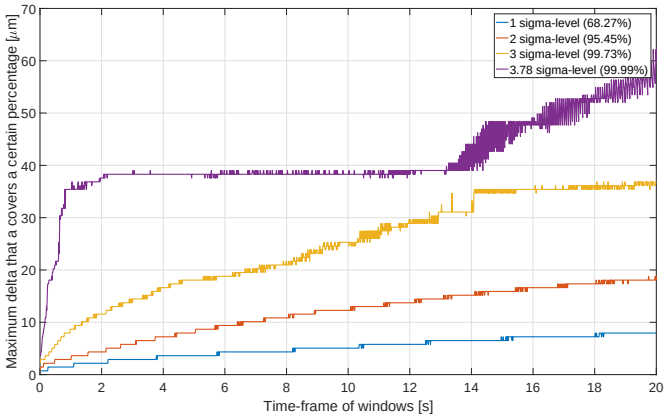

Fig. 5. Maximum occurring delta within an OCP of all occurrences for end-surface positions as a function of the time-length window size.

that needs to be covered. The equation for calculating this standard-deviation is shown in Equation (13).

$$\sigma = \frac{\Delta x_{y\%}}{t_{y\%}} \tag{13}$$

In this equation, σ denotes the standard-deviation. This is equal to the maximum delta that includes $y\%$ of the occurrences, divided by the corresponding sigma-level $t_{y\%}$. σ gives a measure for the variance of a either retina or end-surface, in this case as a function of time without measurement.

3.3 Model noise

The model noise can be interpreted as the possible change of the state, or in this case movement, over time. Since the exact change and time of change is unknown, it is modeled as noise. If no measurements are obtained, the Kalman filter's variance only updates each iteration with Equation (7) as the Kalman gain is zero. The change in variance over multiple samples can then be written as:

$$P_{k|k} = P_{k-N|k-N} + Q_k N \tag{14}$$

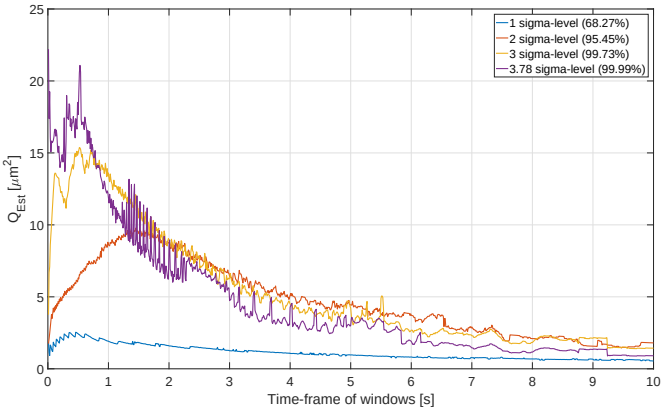

Fig. 6. Estimated Q for retina as a function of time without measurement.

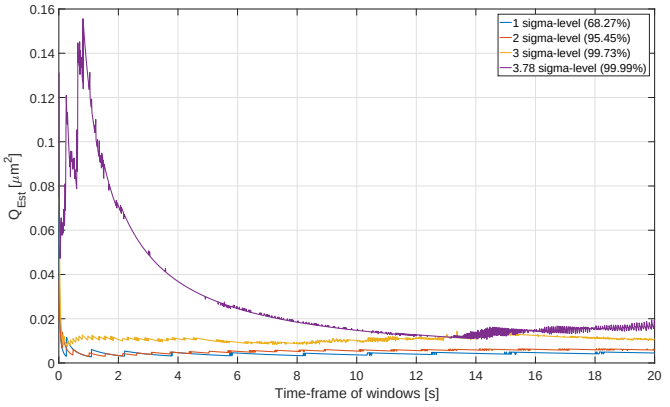

Fig. 7. Estimated Q for end-surface as a function of time without measurement.

In this equation, N is a positive natural number denoting a number of samples without measurement. When only considering the change in variance within this number of samples without measurement, Equation (14) can be simplified to:

$$P_{k|k} = Q_k N \tag{15}$$

The variance can be written as the standard-deviation squared:

$$P_{k|k} = \sigma^2 \tag{16}$$

Substituting Equation (13) and Equation (15) into Equation (16) leads to the following expression:

$$\begin{aligned} P_{k|k} &= \sigma^2 \\ Q_k N &= (\frac{\Delta x_{y\%}}{t_{y\%}})^2 \\ Q_k &= \frac{\Delta x_{y\%}^2}{t_{y\%}^2 N} \end{aligned} \tag{17}$$

The calculated values for Q per time-length and for various coverage percentages are shown in Fig. 6 and Fig. 7.If the data would be normally distributed, the calculated Q for each component would be constant, independent of the time-length and percentage covered. This would then result in a horizontal line in Fig. 6 and Fig. 7.

From visual analysis of Fig. 6 it can be seen that there is no horizontal line for any sigma-level. Although there was much less data available for analysis of the retina, the most likely cause is that the retina movement is not normally distributed. This makes sense as the heartbeat and breathing are not normally distributed. Fig. 7 shows that for sigma-levels 1 and 2, the found values for Q are pretty equal and constant. The jumps that do occur in these lines are due to discretization in the deltas. For the sigma-level three a straight line with an offset with respect to sigma-levels 1 and 2 is shown. This occurs when the data has a heavy tailed distribution. The 3.78 sigma-level shows a non-straight line. This is most likely due the set not being perfectly normal with a heavy tail.

From these figures it can be concluded that the end-surface approximates normal distribution but that it is heavy tailed and that the retina does not seem to be normally distributed at all. However, choosing the maximum occurring value for Q for retina and end-surface, the normal distribution assumption in the Kalman-filter still covers 99.99% of all deltas. The result are model noises of 22.2 and 0.16 micrometer squared for retina and end-surface respectively for a sample frequency of 700 hertz. Since only time-length windows up to 20 for the end-surface and 10 seconds for the retina respectively are analyzed, no guarantees can be given for larger times without looking at that component. For this reason, boundary parameters α and γ from the optimization problem in Equation (3) are equal to 10 and 20 seconds respectively.

3.4 Hardware

Moving the reference mirror from one point to another will always take a certain amount of time, called the travel time t_{tt}. To automatically position the the reference mirror, it is placed on a voice-coil actuator which has a finite acceleration depending on the maximum force that is applied and the mass. This can be seen in Fig. 8. From FRF-measurements it was found that the moving mass was equal to about 350 grams. The maximum force that could be applied given the used amplifier was equal to 20 Newton. From this it results that a maximum acceleration of about 57 meters per second squared could be used. Assuming the coil can deliver infinite jerk, a second-order trajectory generator is added, which uses the maximum acceleration to plan the reference position for the reference mirror. From this second-order trajectory, the expected amount of time required to travel t_{tt} can be determined as a function of the estimated distance between the two detectable components.

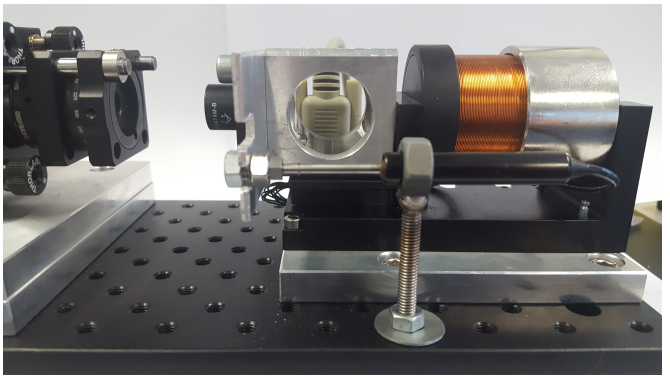

Fig. 8. Voil-coil actuator on which the reference mirror was fixed.

4 Switching behavior

The optimization problem defined stated that the switching solution for current time t, should result in feasible solutions for time going to infinity. Since it is never possible to predict for this length of time iteratively. As mentioned in Section 2, a periodic behavior will occur when switching between the components. Analyzing this behavior in combination with the implemented models, expressions can be found that can be used to simplify the optimization problem. This section discusses the found results and how they can be used to simplify the optimization problem.

4.1 Convergence of variance in periodic behavior

If the number of samples at the retina, number of samples at the end-surface and numbers of samples required for traveling remains constant over time, the switching behavior will be equal. As a result, the variance change on the position of end-surface and retina in a period will also converge to a periodic behavior. This is denoted as follows:

$$\Delta P_{AVisible}(N_A) = \Delta P_{ANotVisible}(N_{tt}, N_B) \tag{18}$$

This equation states that the change in the variance when observing one of the components $\Delta P_{AVisible}(N_A)$, is equal to the change in variance when not observing that component $\Delta P_{ANotVisible}(N_{tt}, N_B)$. As this equation is a function of the Kalman-filter and the periodic behavior, component A can be either retina or end-surface. Component B then denotes the other component. The change in variance on the position when observing component A is a function of the amount of samples observing component A. This can be written as:

$$\Delta P_{AVisible}(N_A) = P_{t_{p_A}} - P_{t_{p_{tA}}}(N_A, P_{t_{p_A}}) \tag{19}$$

In this equation, $P_{t_{p_A}}$ denotes the variance on the position of component A after a first observation of that component after switching. The notation of t_{p_x} was elaborated on in Section 2 and denotes start time of one of the four steps in a period. Observing that component for N_A samples causes the variance to change, resulting in variance $P_{t_{p_{tA}}}$ at time $t_{p_{tA}}$ in a

period at which the mirror starts moving to the other component.

The right hand side of Equation (18) can also be elaborated. This is the part denoting the change in variance on the position when component A is not observed, $\Delta P_{ANotVisible}(N_{tt}, N_B)$. This variable is a function of the amount of samples that component A is not observed $N_{ANotVisible}$. $N_{ANotVisible}$ consists of the travel-time N_{tt} and the time at the other component N_B samples traveling N_{tt} and the amount of samples observing component B as in these cases no observations of component A are made. Since there is no measurement, only the prediction step of the Kalman-filter influences the variance on the position. The resulting variance per iteration was mentioned in Equation (14). The second part of Equation (18) thus becomes:

$$\begin{aligned} \Delta P_{ANotVisible}(N_{tt}, N_B) &= Q_A N_{ANotVisible} \\ &= Q_A(2N_{tt} + N_B) \end{aligned} \tag{20}$$

Since all components on the right half side of Equation (20) are positive real numbers, $\Delta P_{ANotVisible}(N_{tt}, N_B)$ is also a positive real number. Using Equation (18), this means that $\Delta P_{AVisible}(N_A)$ is also a positive real number. This is only possible if $P_{t_{p_A}}$ is larger than $P_{t_{p_{tA}}}(N_A, P_{t_{p_A}})$, given that the variance is always a positive real number.

4.2 Maximal combined variance values

The combined variance on the position is defined as the sum of the variances on position of end-surface and retina, which is thus a variance on the distance between these two components. In a single period, two peaks in the combined variance will occur as can be seen in the example period of Fig. 3. Each peak will occur when arriving at either component, which is N_{tt} samples after leaving the other component. This is because both components are not observed while positioning the mirror. Thus the variance on the position of both components increases. Using the denotation as used in Equation (19) and Equation (20), the values of the variance peaks M_1 and M_2 can be written as:

$$M_x = P_{t_{p_A}} + P_{t_{p_{tB}}} + N_{tt} Q_B \tag{21}$$

From Equation (21), two peaks can be found as component A can be retina or end-surface. Component B then denotes the remainder component.

4.3 Kalman filter convergence

For an infinite number of samples at component A, which can be either end-surface or retina, the Kalman filter's variance will converge to a constant. This value can be found by solving $P_{k|k} \equiv P_{k-1|k-1}$. From the equations for the Kalman filter, it can be found that $P_{k|k}$ can also be written as:

$$P_{k|k} = \frac{R_A(P_{k-1|k-1} + Q_A)}{R_A + P_{k-1|k-1} + Q_A} \tag{22}$$

Solving this equation for $P_{k|k} \equiv P_{k-1|k-1}$ results in an expression for converged constant $P_{A,conv}$:

$$P_{conv} = \frac{-Q_A \pm \sqrt{Q_A^2 + 4R_A Q_A}}{2} \tag{23}$$

Thus, when the time at a component is large enough, it can be assumed that $P_{t_{p_{tA}}}$ is equal to the converged value $P_{A,conv}$. Since it is not possible to find a direct expression for the Kalman filter's position after N samples this value has to be determined iteratively, which is a computationally heavy process for large values of N. To limit this computation time, the converged value $P_{A,conv}$ can be used instead.

5 Supervisor

To maximize the percentage of time at the retina in a single period as denoted in Equation (1), it is desired to obtain a small value for the time at the end-surface, and a large value for the time at the retina. To obtain an expression for the time, or in this case amount of samples, at the retina, Equation (18) is rewritten to obtain Equation (24).

$$N_{ret} = \frac{P_{t_{pes}} - P_{t_{ptes}}(N_{es}, P_{t_{pes}}) - 2Q_{es}N_{tt}}{Q_{es}} \tag{24}$$

When maximizing N_{ret}, the amount of samples at this component, $P_{t_{pes}}$ should be maximal and $P_{t_{ptes}}$ should be minimal.

We assume that the amount of samples at the retina is sufficiently large for the variance of the Kalman filter tracking the retina to converge. One of the two peaks in a period can then be written as:

$$\begin{aligned} M_1 &= P_{t_{pes}} + P_{t_{ptret}} + N_{tt} Q_{ret} \\ &= P_{t_{pes}} + P_{ret,conv} + N_{tt} Q_{ret} \end{aligned} \tag{25}$$

Since the travel time t_{tt} is determined from the hardware, trajectory planner and the estimated distance between retina and end-surface, the only remaining free variable is the start value of the end-surface $P_{t_{pes}}$. The value of both peaks should remain bounded under boundary value β. Since a higher value for $P_{t_{pes}}$ results in a time for observing the retina, Equation (25) can be used to find an expression for the maximum value for $P_{t_{pes}}$, $P_{t_{pes},max}$.

$$\begin{aligned} P_{t_{pes},max} + P_{ret,conv} + N_{tt} Q_{ret} &= \beta \\ P_{t_{pes},max} &= \beta - P_{ret,conv} - N_{tt} Q_{ret} \end{aligned} \tag{26}$$

Using this value, the end value for the end-surface $P_{t_{ptes},max}$ can be determined for a given N_{es}. Given these two variables, it can be check if the other peak value exceeds the boundary condition under these conditions. If not, the found solution is feasible. Using Equation (24) and Equation (26), the maximum value for N_{ret} can be found as a function of boundary

value β, N_{tt} and N_{es}. With N_{ret} and N_{ret} known, the percentage of time at the retina can be determined for a period in which the variance shows periodic behavior.

This same process can be repeated for the second peak M_2. This peak can be written as:

$$M_2 = P_{t_{pret}} + P_{t_{ptes}} + N_{tt} Q_{es} \tag{27}$$

If it is assumed that the system is converged to periodic behavior in combination with sufficiently large amount of samples at the retina, then Equation (27) can be written as:

$$\begin{aligned} \Delta P_{retVisible}(N_{ret}) &= \Delta P_{retNotVisible}(N_{tt}, N_{es}) \\ P_{t_{pret}} - P_{t_{ptret}}, P_{t_{pret}}) &= Q_{ret}(2N_{tt} + N_{es}) \\ P_{t_{pret}} - P_{ret,conv} &= Q_{ret}(2N_{tt} + N_{es}) \\ P_{t_{pret}} &= Q_{ret}(2N_{tt} + N_{es}) + P_{ret,conv} \end{aligned} \tag{28}$$

This equation shows that $P_{t_{pret}}$ depends on N_{es} and N_{tt}. Since N_{tt} is determined as a function of the distance between the two components and the trajectory planner, this value can not be chosen arbitrarily. If Equation (28) is substituted into the equation for peak M_2, Equation (27), it can be rewritten to:

$$\begin{aligned} M_2 &= P_{t_{pret}} + P_{t_{ptes}} + N_{tt} Q_{es} \\ &= Q_{ret}(2N_{tt} + N_{es}) + P_{ret,conv} + P_{t_{ptes}} + N_{tt} Q_{es} \end{aligned} \tag{29}$$

Setting this peak value equal to the boundary condition value, maximal value $P_{t_{ptes},max}$ can be found. For arbitrary number for N_{es}, the maximal value $P_{t_{pes},max}$ can be found as well. From these values once again the amount of samples at the retina can be determined, and thus also the percentage of time at the retina.

Using peaks M_1 and M_2, two values for N_{ret} can be found for an arbitrarily chosen N_{es}, N_{tt} and boundary value β. From these two values for N_{ret}, the highest should be executed as this will result in the highest percentage of time at the retina.

This process can be repeated for increasing amounts of N_{es}, until a maximum in the percentage of time at retina as a function of N_{es} is found. These values for N_{es} and N_{ret} denote the switching behavior that should be used, as these provide the maximum percentage of time at retina for a given N_{tt} and β.

Determining the switching strategy using this set of equations thus solves optimization problem Equation (3). Since periodicity in the Kalman filters was assumed, finding a feasible combination of samples at end-surface and samples at retina results in a feasible combination for time going to infinity. Furthermore, this method only holds if the amount of samples at the retina is sufficiently large, as the converged value for the variance of the retinas' Kalman filter was used. For small N_{ret}, it can not be guaranteed that the end value $P_{t_{ptret}}$ approximates $P_{ret,conv}$. Since N_{ret} has to be calculated for various N_{es} to find the optimal result, the supervisor is computationally low cost for small N_{es}.

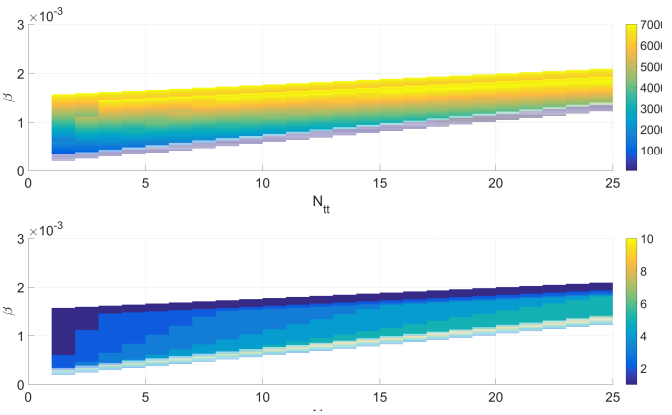

Fig. 9. Lookup-table created from set of equations of supervisor. a) Optimal N_{ret} as a function of β and N_{tt}. b) Optimal N_{es} as a function of β and N_{tt}.

5.1 Implementation

Using the set of equation determined for calculating the optimal N_{es} and N_{ret} as a function of N_{tt} and β can be done real-time. However, due to computation time this may not be possible. Also, it doesn't scale with the software execution frequency. The computation cost remains equal if the software execution frequency is increased, resulting in problems at a certain frequency.

Creating a lookup-table can provide a solution. Calculating N_{ret} for various values for N_{es}, β and N_{tt}, an optimal mapping can created for N_{es} and N_{ret} as a function of N_{tt} and β. The created lookup-table can be loaded when starting the software, after which the best solution can easily be looked up. Doing so for the given retina and end-surface parameters, the following lookup-table is obtained.

This lookup-table is generated beforehand and since the optimal solution only has to be looked up, it is low cost. However, it is currently assumed that certain parameters are constants. If these parameters would become variables, the lookup-table method does not hold anymore. For instance, it is currently assumed that the model noise on the position of the retina is a constant value. However, it is well possible that this value can be altered once a reliable dynamic model is obtained.

To cope with these parameters being variable, two solutions are available. Either real-time execution can be done, or multiple lookup-tables have to be generated for various parameter configurations. This thus provides a a trade-off. In the current implemented software these parameters are still constants. Since the initially implemented set of equations for determining the best solution was a factor 10 larger than the available computation time for 700 hertz, it was decided to use the lookup-table implementation for simulations and experiments.

6 Simulations

The supervisor as discussed in Section 5 is based on the assumption of the Kalman filters having converged to peri-

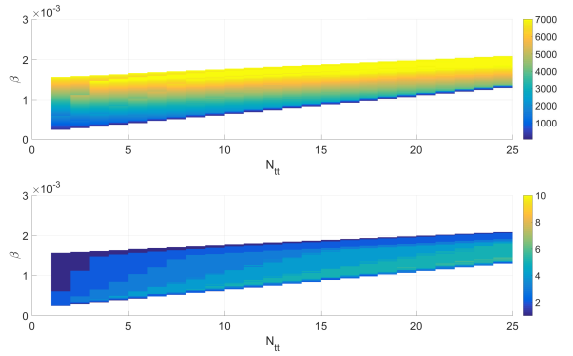

Fig. 10. Lookup-table created from brute force simulations. a) Optimal N_{ret} as a function of β and N_{tt}. b) Optimal N_{es} as a function of β and N_{tt}.

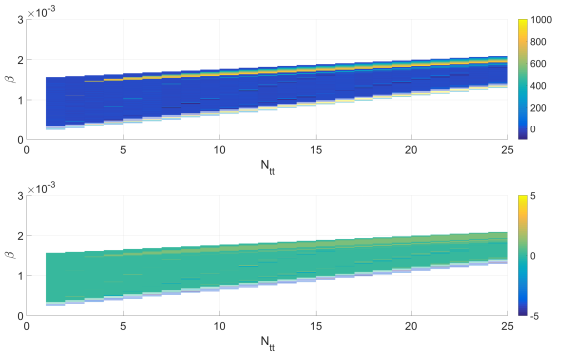

Fig. 11. Difference in lookup-tables of brute force simulations and from supervisor. a) Optimal N_{ret} as a function of β and N_{tt}. b) Optimal N_{es} as a function of β and N_{tt}.

odicity and large values for N_{ret}. Since during surgery the distances to the retina change due to movement of the instrument and due to movements of end-surface and retina, the system may not be in perfect periodicity as $\Delta P_{ANotVisible}$ of Equation (18) is dependent on N_{tt}. Furthermore, it can be checked if the supervisor algorithm provides the optimal solution within a solution space, by comparing it to a brute force algorithm. . This solution space concerns values of N_{ret} and N_{es}, being bounded by the sample frequency and boundary values α and β.

6.1 Supervisor validation

To check if the supervisor provides the optimal solution to the optimization problem of Equation (3), a second mapping of the optimal N_{ret} and N_{es} as a function of N_{tt} and β was created. This mapping was created with a brute force algorithm, testing the obtained β for various values of N_{ret}, N_{es} and N_{tt}. Since β is computed as a function of N_{ret} rather then the other way around, using the brute force algorithm in real-time is a computationally expensive and inefficient way to find the optimal solution. The resulting mapping of this brute force method is shown in Fig. 10. Comparing the difference in optimal solutions for the brute force- and the supervisor lookup-tables results in Fig. 11. Comparing the two tables shows that the mapping of the retina have an average difference 105 samples with a standard-deviation of 258.52 samples. 80% of all compared values in the feasible domain showed a difference in samples equal or smaller then 100. The end-surface comparison shows an average difference of 0.5 samples with a standard-deviation of 0.9 samples. 80% of the compared values has no difference in optimal amount of values. The largest differences in samples for the retina lookup-tables occur for large values of β and large values of N_{tt}. These is an area where N_{ret} is expected to be large. The likely cause of this is the iterative step-size used to find $P_{t_{p_{ret}}}$ from $P_{t_{p_{tret}}}$ in the supervisor, as it is assumed that the brute force solution is perfect. Due to time limitations, this could not be validated. Since staying an additional amount of samples at a component, it is possible that the variance of the distance between the components will exceed the boundary

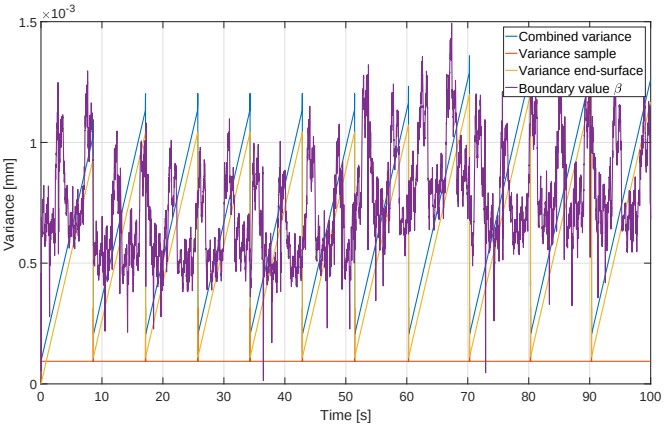

Fig. 12. Simulation results for supervisor testing for distance between instrument tip and retina of 0.1 millimeter, with movements of end-surface and retina.

value. From this it can be concluded that the supervisor will exceed the boundary under certain static conditions.

6.2 Supervisor validation for moving components at small distances

When close to the retina, it is essential to keep the variance bounded to prevent accidental touchings of the retina. Simulations were done for small distances between end-surface and retina with and without these components moving. To mimic the movements of retina and end-surface, position data from the clinical trials was used. The results of the simulation with moving retina and end-surface are shown in Fig. 12. This figure shows that the system was unable to keep the variance on the distance between instrument tip and retina bounded below β. To determine the cause of this failure, the hypothesis that this behavior was caused by the moving components was tested. The same simulation was done without the movements of the retina and end-surface, thus having a constant distance between the components. The resulting behavior from this simulation is shown in Fig. 13. In these simulations, the system was able to keep the uncertainty bounded under β. This confirms the hypothesis that the

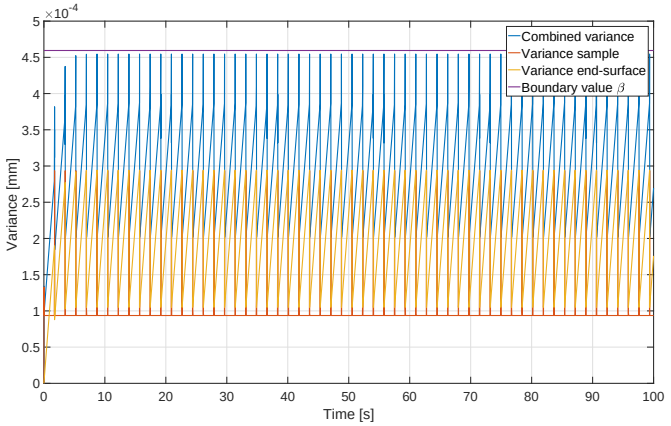

Fig. 13. Simulation results for supervisor testing for distance between instrument tip and retina of 0.1 millimeter, without movements of end-surface and retina.

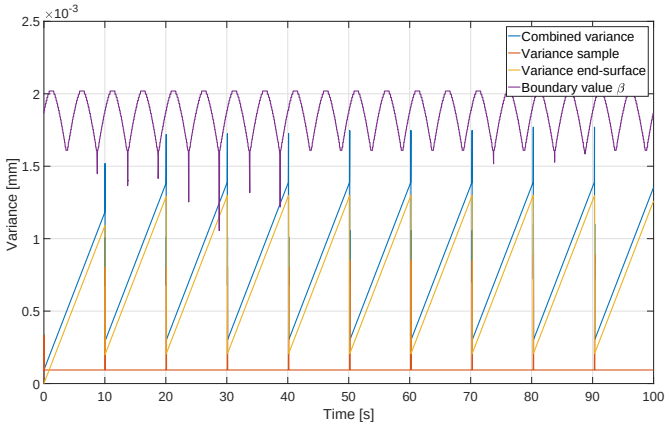

Fig. 14. Simulation results for supervisor testing for distance between instrument tip and retina of 0.1 millimeter, with movements of end-surface and retina and surgical instrument.

movements caused the boundary to be violated. However, since movements of the retina were accounted for in determining β, it is likely that the assumption of periodicity does not any longer. The supervisor already expects the Kalman filters to have the maximum and minimum value from periodicity, to which the filters could not have converged yet.

6.3 Supervisor validation for moving components at long distances

Besides testing at small distances, it was also tested how the supervisor responds and copes with larger movements. Therefore the simulations as done in the previous subsection were repeated, but now for larger distances. The eye has an approximate diameter of 24 to 25 millimeter [2], therefore simulations where done in which the surgeon operates with a sine movement inside the eye. A sine with an amplitude of 9.75 millimeters, and frequency of 0.2 hertz, was applied at a general distance of 10 millimeter. The result is shown in Fig. 14. From this figure it can be seen that the supervisor is able to keep the variance bounded for the largest part of the eye, even if there are movements of the end-surface, retina and surgical instrument. From this it can be concluded that especially for very small distances it is difficult to keep the variance bounded. From the lookup-tables this could also be observed, as even for a travel time of 1 sample, some boundary values are unfeasible to obtain. In these cases, the supervisor can will try to obtain the best possible feasible solution. However, it is essential to feed this information back to the system, so that the surgeon can be alerted that the supervisor is unable to provide a 99.99 certainty. If the distance from instrument tip to end-surface is known, it can also be computed until which distance optimal performance can be achieved.

7 Experiments & Validation

In simulation an ideal world is represented in which components are detected instantly and positioning the mirror is ideal. These ideal situations may not hold in a real environment. For this reason, experiments were performed to find if the ideal environment of the simulation is a valid representation of the reality, or if other influences need to be taken into account.

For these experiments, the hardware as discussed in subsection 3.4 was used. The sample arm of the SD-OCT was connected to the optical probe, measuring the location of a piece of paper. The conducted experiments were done to verify the supervisor's behavior in a real environment.

7.1 Supervisor experiments in real environment

To test the switching behavior, the lookup-tables that were created with brute force simulations in Section 6 were used to test the concept of a supervisor in the real environment. Based on the estimated distance between end-surface and the paper, the boundary value β and N_{tt} could be determined. Using these values, N_{ret} and N_{es} could be obtained from the lookup-table. The reference mirror was set to position itself such that the observable component would lie at 1 millimeter from the start of the measurement window. This position is arbitrary since no research has been done on optimal positioning of the reference mirror. Optimizing the positioning of the mirror results in a lower N_{tt} for equal distance. As a result, the time in which there are no observations is smaller, enhancing performance. Since the sample enters the A-scan from the end of the measurement window, it may not be required to move it all the way to the front of the window for detection. For fixed position of the sample, experiments have been conducted to validate that also in a real environment it is possible to maximize the time at the sample, whilst keeping the variance on the distance bounded under β. Fig. 15 shows the Kalman filter's variances, and combined variance, over time during an experiment where the distance between end-surface and paper was approximately 14 millimeter. The travel time N_{tt} corresponding to this distance is 24 samples. A close-up of a single period is shown in Fig. 17. Although not clearly visible in Fig. 15, only one of the two peaks of each period exceeds boundary value β. Plot (a) of Fig. 16 shows the delta between the peak values and the β. From analysis of the cause of these peaks exceeding β, two

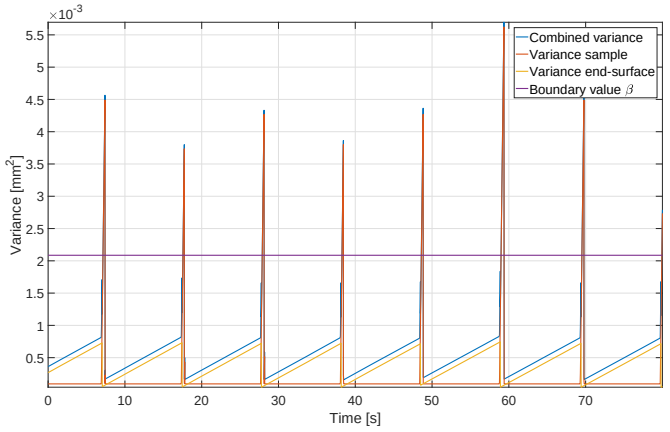

Fig. 15. Variances obtained during experiments for estimated distance between sample and end-surface of about 14 millimeter.

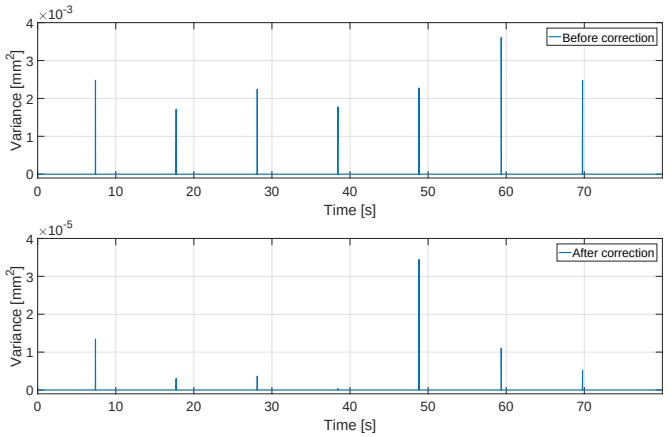

Fig. 16. a) Delta between peak values of combined variances as obtained during measurements and β. b) Delta between peak values of combined variances as obtained during measurements and β after compensation.

causes were found:

1. The travel time N_{tt} appeared to be 49 samples instead of the expected 24 samples. This difference is the result of communication delay and overshoot of the reference mirror, as can be seen in Fig. 17. Plot (a) of this figure shows the system state which denotes the state of what the supervisor is doing. Plot(b) shows the mirror-position and desired mirror-position. In this figure the commutation delay can be recognized, as the response in mirror-position is a few samples after the system-state changes. The overshoot is also visible in plot (b). This overshoot is due to a low-performance controller. Improving the controller was not possible without the system becoming unstable due to a imperfect non-linearity compensation.
2. The detection software did not instantly recognize the component after positioning of the reference mirror. This resulted in an additional amount of samples without detection. After compensating for the travel time N_{tt}, retina detection required on average 128 additional samples before detection. The end-surface detection was instant.

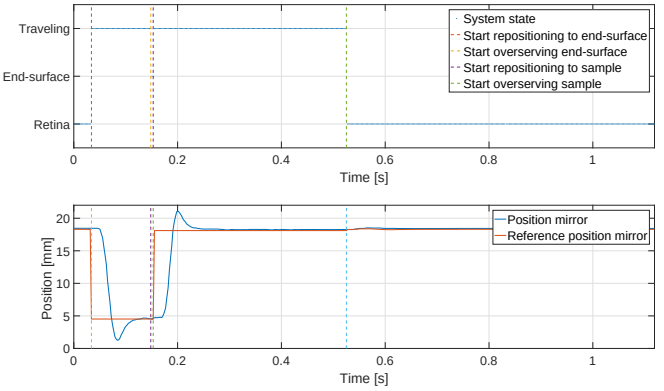

Fig. 17. a) System state for a single period. b) Mirror position corresponding to the period of plot a.

From the adjusted travel time, a corrected value for β was determined using the executed N_{ret} and N_{es}. Compensating for the additional amount of samples required before detection, using Equation (15), values were fond for variance peak values without this delay. The result of this compensation is shown in plot (b) of Fig. 16. The peak values now are now much closer to the actual boundary, differentiating only 6 percent from the expected β. From this it was concluded that the calculated travel time is wrong and that the additional samples required before detecting a component are the main cause of the original peak values being much larger than the boundary value. The samples due to communication delay and position overshoot should be able to be resolved or determined. In case these values are determined, these can be added as additional samples required for traveling. Improving the detection software would result in a faster detection of the components. Since the amount of samples can not be determined beforehand, the supervisor can not compensate for this. A possible solution is to determine a maximum or average amount of samples required and add these to the travel time. This way a better approximation can be made of how many samples are required until the next component will be detected. Due to time limitations and the absence of the device, it was not possible to repeat the experiments using the adjusted travel time.

Finally, it was found that the execution-rate of the software was not equal to the set 700 hertz, but more closely due to 430 hertz. For the results of these experiments this does not matter much, except that the expected travel time should thus be 15 samples. From this it can be concluded even further that the position controller should be improved. It should be researched further why the execution rate of the software is this value and how it can be increased. Since the model noise was determined for 700 hertz, execution on lower frequencies causes the variance to be lower than it should actually be after that time. During operation in surgery, it should be checked that the execution rate is at least 700 hertz, as otherwise dangerous situations could show.

8 Conclusions & Recommendations

In this work, an automatically moving reference mirror was introduced to increase the measurement window for an SD-OCT device with limited measurement range. Moving the reference mirror results in a shift of the entire measurement window. This enables component detections at distances larger than the size of the measurement window, thus making it possible to track the position of the retina from any position of the instrument in the eye. This makes it possible to construct model of the sample, use a larger variety of surgical instrument and validate the functioning of the SD-OCT from larger distances. To ensure safety and maximize performance, a strategy for positioning the reference mirror was formulated in the form of an optimization problem. The optimization problem maximizes the average time at the sample whilst keeping the maximum variance on the distance to the sample bounded, such that it can be guaranteed with 99.99% certainty that the instrument tip is not touching the sample, for each moment from the current time to infinite. To this end, two Kalman filters were introduced to track the positions of both end-surface and retina. From analysis of clinical data, the model noise for each Kalman filter was determined for both end-surface and retina. Since simulation for time going to infinity is impossible, it was assumed that the distance between sample and end-surface remains constant over time. This way the Kalman filters' variance change in a period becomes constant, thus being equal for all upcoming periods, which resulted in a relaxation for the solution time. Having only to optimize for one period, expressions were found for the variance peaks in a single period. Since it was desired to achieve large times at the sample, it was assumed that after observing the sample, the variance approximated a converged value which could be determined beforehand. Using the assumptions mentioned and the expression for the variance peak values, a supervisor was constructed. The supervisor could be used real-time, if the computation time of a solution would not exceed the execution time of the software. If the latter would be the case, the supervisor could be used to construct a lookup-table, from which the amount of samples at a component follow from the travel time and boundary value. Comparing the supervisor with a brute-force optimization algorithm showed differences in estimated optimal value. Since the predicted values of the supervisor were occasionally higher than of the brute force algorithm's lookup-table, this could result in exceeding the boundary value. Further research is required to find the exact cause of these differences. From simulations it was concluded that the supervisor functions well for most distances between the components, but is unable to keep the uncertainty bounded for small distances between the components when there are movements involved. The expected cause for exceeding the boundary is that the periodicity assumption does not hold. For small distances, the supervisor will thus not be able to guarantee the 99.99% certainty. However, simulations also showed that for most distances in the eye, safe operation can be guaranteed whilst observing the retina for long periods of time. To validate the functioning of the supervisor in a real environment, experiments were conducted. From these experiments it was concluded that overshoot in the actuator, communication delay and a delay in the detection algorithm, caused the actual travel time to be longer than expected. Compensating for these additional samples was done and the expected boundary value was obtained. It is recommended to find expressions for these delay and to incorporate them into the travel time. This way the supervisor should be able to handle the non-ideal environment.

References

[1] Optical and Biomedical Engineering Laboratory and University of West Australia, Introduction to OCT, `http://obel.ee.uwa.edu.au/research/fundamentals/introduction-oct/`, Online; accessed 30-10-2019

[2] Kolb, H., Fernandez, E., Nelson, R., The Organization of the Retina and Visual System, University of Utah Health Sciences Center, Salt Lake City (UT), Last updated: 19-03-2018

[3] Podoleanu, A. Gh., Optical coherence tomography, Journal of Microscopy, volume: 247(3), pages: 209-219, year: 2012, month: September

[4] Drexler, W., Fujimoto, J.G. and Editors, Optical Coherence Tomography Technology and Applications, Springer, year: 2008, ISBN: 978-3-540-77549-2

[5] Kalman, R. E., A New Approach to Linear Filtering and Prediction Problems, Journal of Basic Engineering, year: 1960

[6] Galanis, G., Anadranistakis, M., A one-dimensional Kalman filter for thecorrection of near surface temperature forecasts, Meteorol, year: 2002

[7] Coerver, L.T., Douven, Y.G.M., Molengraft, M.J.G. van de, B-Spline Surface Modelling with Coverage Path Planning towards Autonomous Vitrectomy, Master thesis, year: 2018, month: November

Technische Universiteit
Eindhoven
University of Technology

Declaration concerning the TU/e Code of Scientific Conduct for the Master's thesis

I have read the TU/e Code of Scientific Conduct[i].

I hereby declare that my Master's thesis has been carried out in accordance with the rules of the TU/e Code of Scientific Conduct

Date

02-10-2019

Name

M.C.W. Schooten

ID-number

0869793

Signature

MCWSchooten

Submit the signed declaration to the student administration of your department.

[i] See: http://www.tue.nl/en/university/about-the-university/integrity/scientific-integrity/
The Netherlands Code of Conduct for Academic Practice of the VSNU can be found here also.
More information about scientific integrity is published on the websites of TU/e and VSNU